

Thermally detected EPR studies of Cr^{3+} ions in GaP

J. L. Dunn and C. A. Bates

Physics Department, The University, Nottingham, NG7 2RD, United Kingdom

M. Darcha, A. Vasson, and A-M. Vasson

*Laboratoire de Physique des Milieux Condensés, Physique 4, Université de Clermont-Ferrand II**Boîte Postale 45, 63170 Aubière, France*

(Received 27 August 1985; revised manuscript received 15 October 1985)

From an analysis of the ground-state energies of the 1.03-eV zero-phonon optical line in chromium-doped GaP crystals, an effective Hamiltonian appropriate to Cr^{3+} ions is produced. It is shown that some of the lines seen in thermally detected EPR spectra can be accounted for from strain-stabilized sites in this model whilst further lines arise from sites with zero strain.

In 1977, Krebs and Stauss¹ were able to identify the Cr^{3+} ion in GaAs by electron-paramagnetic-resonance (EPR) techniques. This paved the way to the understanding of the much-studied and -used chromium-doped GaAs system.² In contrast, the behavior of chromium-doped GaP is poorly understood² although many EPR studies have been carried out. So far substitutional Cr^{1+} (Ref. 3) and Cr^{4+} (Ref. 4) have been positively identified but many other very complicated lines exist. Recently,⁵ a Cr^{2+} center was also identified by thermally detected (TD) EPR techniques. (An orthorhombic Cr^{3+} center has also been reported⁶ but it is believed now that this center is not substitutional Cr^{3+} .²)

We report new TD-EPR experiments from which we detect the substitutional Cr^{3+} ion for the first time. Our analysis correlates the center with the ground states of the 1.03-eV zero-phonon line (ZPL) seen in both absorption⁷ and luminescence.⁸

The TD-EPR data have been obtained at liquid-helium temperatures with magnetic fields \mathbf{B} in the range 0–3 T.

Several semi-insulating crystals (from MCP Ltd. and The Siemens Company) have been studied. Placing the sample in the waveguide enables us to obtain results at frequencies between 8.0 and 12.4 GHz and the technique is particularly sensitive to strongly coupled ions.⁹

Figures 1 and 2 show typical sets of results with \mathbf{B} rotated in the $(1\bar{1}0)$ and (111) planes at 9.3 GHz. Spectra in other planes and at other frequencies have also been obtained. The lines previously identified⁵ as being due to a Cr^{2+} center are indicated. Note also that many experimental points are shown connected as a guide.

We begin our analysis with the 1.03-eV ZPL. Eaves, Halliday, and Uihlein¹⁰ studied the angular dependence of their Zeeman experiments which indicated that an $S = \frac{3}{2}$ ion is present in GaP:Cr crystals. As the data are chromium related, they suggested that they were observing a Cr^{3+} center, with a 4T_1 ground state. The excited state involves two doublets split by 1.20 meV (9.7 cm^{-1}).

In contrast to Eaves *et al.*¹⁰ (who analyze Zeeman data)

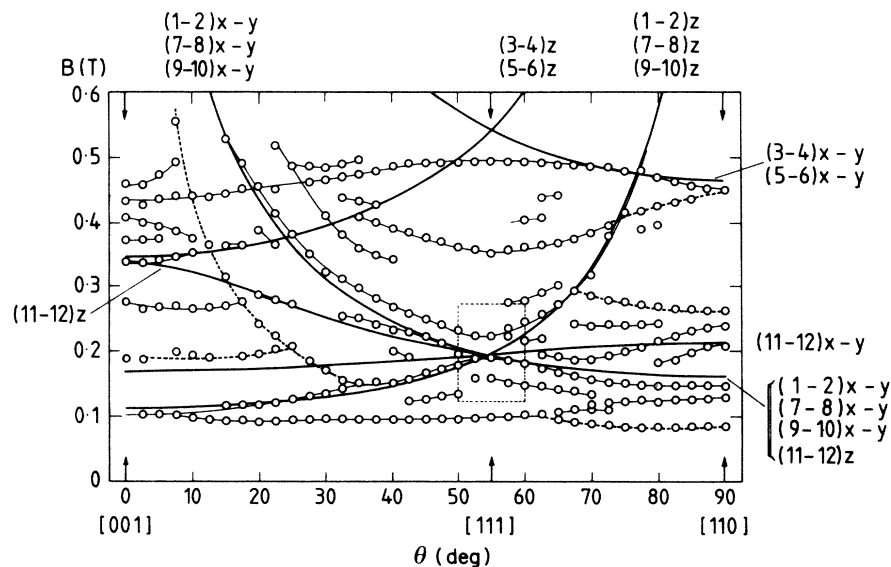


FIG. 1. A plot of the TD-EPR spectra for a sample (No. V772E), from the Siemens Co. for \mathbf{B} in the $(1\bar{1}0)$ plane at 9.3 GHz and liquid-helium temperatures. Where experimental points (\circ) can be connected, they are indicated by fine solid lines. Points previously identified as Cr^{2+} (Ref. 5) are connected by dashed lines. The theoretical strain-stabilized isofrequency curves are given by heavy solid lines and labeled according to the levels between which the transition occurs and the symmetry of the site involved.

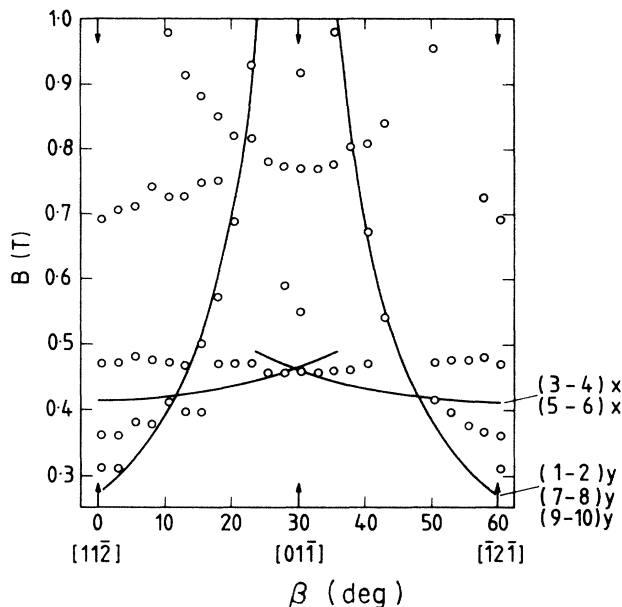


FIG. 2. A plot of the TD-EPR spectra from the same sample as in Fig. 1 for \mathbf{B} in the (111) plane at 9.3 GHz. Notation as Fig. 1.

we first look at the zero-field data to produce a ground-state energy-level scheme in zero field consisting of doublets at

$$0, 0.27, 0.43, 1.01, 1.17, \text{ and } 1.34 \text{ meV} \quad (1)$$

(each with an error of ± 0.2 meV). This is a revised form of the splittings given originally by Williams *et al.*⁸ The above suggests an effective ground-state Hamiltonian for a typical ion in terms of the effective orbital angular momentum ($l=1$) of the form¹¹

$$\mathcal{H}_{\text{eff}} = \gamma \lambda k_1^T \mathbf{l} \cdot \mathbf{S} + \mathcal{H}_{2\text{SO}} + \alpha l_z^2, \quad (2)$$

where

$$\mathcal{H}_{2\text{SO}} = \lambda [c(E_\theta E_\delta^z + E_\epsilon E_\epsilon^z) + b(\mathbf{l} \cdot \mathbf{S})^2] \quad (3)$$

represents second-order spin-orbit coupling. αl_z^2 is the z-type tetragonal random strain [$\alpha = (2/3)V_E \bar{Q}_\theta$] and (for the \hat{z} axis along [001])

$$E_\theta = \frac{1}{2}[3l_z^2 - l(l+1)], \quad E_\epsilon = \frac{\sqrt{3}}{4}(l_+^2 + l_-^2). \quad (4)$$

E_δ^z is E_θ with l replaced by S , etc., k_1^T is the isomorphic constant ($= -3/2$), λ ($= 83 \text{ cm}^{-1}$) is the spin-orbit coupling constant,¹¹ and γ is the first-order Jahn-Teller $T \otimes e$ reduction factor together with other second-order spin-orbit contributions involving $\mathbf{l} \cdot \mathbf{S}$. The parameters b and c involve second-order Jahn-Teller and crystal-field terms. Sites with x- or y-type strain may also be described by Eq. (2) if z is replaced by x , y with $\alpha = [-(1/3)\bar{Q}_\theta + (\sqrt{1/3})\bar{Q}_\epsilon]V_E$, and $[-(1/3)\bar{Q}_\theta - (\sqrt{1/3})\bar{Q}_\epsilon]V_E$, respectively.

Two sets of the parameters γ , b , c , and α have been found satisfying (1), viz.,

$$\begin{aligned} \gamma &= 0.0121 \pm 0.0007, & b &= -0.0009 \pm 0.0012, \\ c &= 0.0035 \pm 0.0025, & \alpha &= -3.3 \pm 0.8 \text{ cm}^{-1}, \end{aligned} \quad (5)$$

and

$$\begin{aligned} \gamma &= -0.0114 \pm 0.0004, & b &= -0.0024 \pm 0.0014, \\ c &= -0.0114 \pm 0.0012, & \alpha &= -3.9 \pm 0.35 \text{ cm}^{-1}. \end{aligned} \quad (6)$$

The first fit is preferred on physical grounds because first-order contributions to γ must be positive and any negative second-order terms are most unlikely to wipe out the first-order term, particularly as b and c are negative. (This follows from evaluating all contributions to b and c including terms other than 4F .¹²)

In a Jahn-Teller model the effective Hamiltonian for the magnetic field terms is

$$\mathcal{H}_B = \mu_B \mathbf{B} \cdot (\gamma k_1^T \mathbf{l} + 2\mathbf{S}) + H_{2\text{OZ}}, \quad (7)$$

where

$$\begin{aligned} \mathcal{H}_{2\text{OZ}} &= \mu_B \{ [2c(\mathbf{B} \cdot \mathbf{S}) + (E_\theta E_\theta^{SB} + E_\epsilon E_\epsilon^{SB})] \\ &\quad + b[(\mathbf{l} \cdot \mathbf{S})(\mathbf{l} \cdot \mathbf{B}) + (\mathbf{l} \cdot \mathbf{B})(\mathbf{l} \cdot \mathbf{S})] \}, \end{aligned} \quad (8)$$

and

$$E_\delta^{SB} = \frac{1}{2}(3B_z S_z - \mathbf{B} \cdot \mathbf{S}), \text{ etc.}$$

Assuming we describe the excited states as did Eaves *et al.*¹⁰ the predicted optical ZPL Zeeman (OZ) pattern is in very good agreement with the data especially for the preferred fit (5). It is an improvement on the parameters given by Eaves *et al.*¹⁰ which are equivalent to

$$\gamma = 0.027, \quad b = -0.0097, \quad c = 0.0032,$$

with strain described by δS_z^2 with $\delta = -0.09 \text{ meV}$ (-0.73 cm^{-1}).

Having fitted the optical ZPL, we now try to predict the EPR results from our fit (4) to optical work. Note, however, that there is no reason why the value of α needed to fit the EPR data should be the same as that for the ZPL peaks. For optical transitions, $\alpha = -3.3 \text{ cm}^{-1}$ can be interpreted as the value of strain at which the intensity of transitions between ground (4T_1) and excited (4T_2 or 4A_1) states is a maximum; α need not be the same for EPR transitions within 4T_1 . All centers must be considered and they are subjected to various random strains dominated by those of E -type symmetry. Intensity calculations are needed to determine which strains dominate the EPR spectra.

Figure 3 shows the zero-field energy level pattern as a function of α for z-type strains. The arrow indicates the position of the zero-field fit (5) for optical work. Experimentally we propose that EPR peaks will be observed either (a) where the product of transition intensity versus α and the strain distribution function is a maximum (most probably at zero strain) or (b) when resonances from different strain sites superpose.

Computer calculations show that sites of negative strain obey condition (b) for all α less than -20 cm^{-1} . These EPR lines are said to be strain stabilized and are potentially strong as many sites contribute to them (positive strain sites do not become stabilized until physically unrealizable strains). The computer-predicted isofrequency curves for the (110) and (111) planes at 9.3 GHz from these (negative) strain-stabilized sites are shown in Figs. 1 and 2. The predominant states for each energy level are shown in Fig. 4. The computed predictions for the (110) plane can be explained, to a first approximation, by considering the splitting

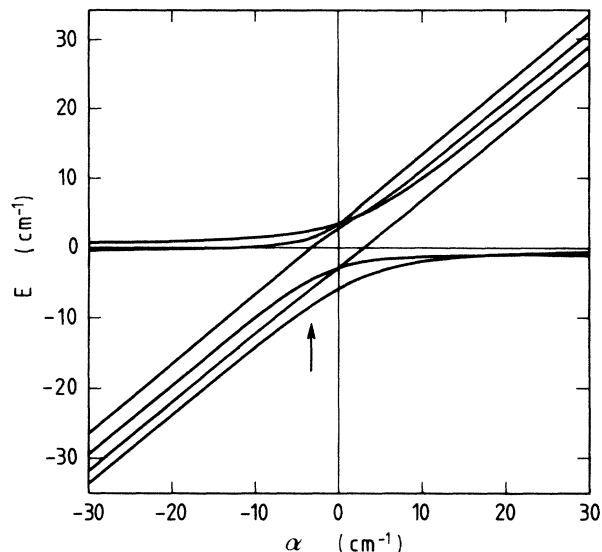


FIG. 3. The energy-level pattern for the ⁴T₁ ground state as a function of E_θ-type strain for fit (5).

of the doublets by $g\mu_B\mathbf{B}\cdot\mathbf{S}$ with $g=2$. This predicts isofrequency curves for z sites between doublets containing $m_s = \pm 3/2$ (namely, 1-2, 7-8, and 9-10) described by

$$B = B_0 \sec\theta \quad (9)$$

where $B_0 = 0.115$ T for $\nu = 9.3$ GHz. Similarly the z -site 3-4 and 5-6 ($m_l = \pm 1, m_s = \pm \frac{1}{2}$) transitions are given by

$$B = 3B_0 \sec\theta \quad (10)$$

Finally, the z site 11-12 transition ($m_l = 0, m_s = \pm \frac{1}{2}$) is given by

$$B = 3B_0(4 - 3\cos^2\theta)^{-1/2} \quad (11)$$

(The formula is different for this transition because it is

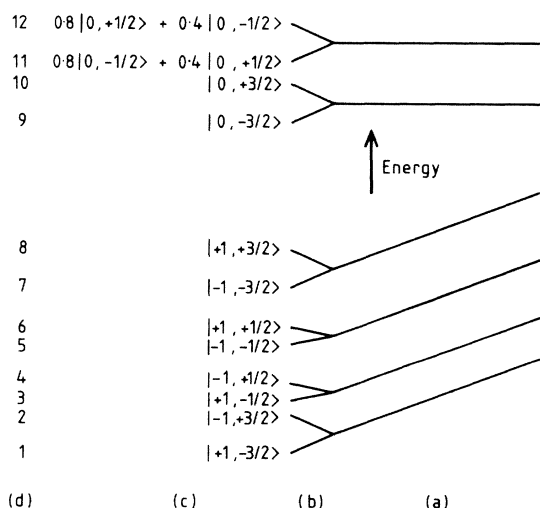


FIG. 4. Schematic energy-level diagram of (a) negative strain-stabilized sites showing (b) splittings in a magnetic field, (c) approximate eigenstates in terms of $|m_l, m_s\rangle$, and (d) the level labels.

only with $m_l = 0$ and $m_s = \pm \frac{1}{2}$ that S_x and S_y in $g\mu_B\mathbf{B}\cdot\mathbf{S}$ contribute to the energy splitting to this approximation.)

Curves for x and y sites are obtained from (9), (10), and (11) by symmetry arguments. Note that the experimental spectra (Fig. 1) show both the required $\sqrt{2}$ factor between the resonance fields for \mathbf{B} along [001] for z sites and B along [110] for x - y sites and the factor of 3 between lines attributed to Eqs. (9) and (10).

The differences between the computer calculations and this simple explanation, namely, that the z -type isofrequency curves cut the [110] axis at finite, rather than infinite, values of B , is that, because the eigenstates are not the pure states (shown in Fig. 4) given by a first approximation, S_x and S_y will have small contributions to the lines. This also means that lines predicted to be coincident by (9) or (10) will separate as the field increases. However, they could not be resolved experimentally so their mean is displayed.

The strongest resonances seen experimentally in the (111) plane fit the predicted (1-2)_y, (7-8)_y, and (9-10)_y strain-stabilized isofrequency curves very well (Fig. 2). The fit is also good in the (1 $\bar{1}$ 0) plane (Fig. 1), except for near the [111] direction where some deviations occur. Three peaks are observed in the region of $B = 0.2$ T near [111]. The middle one coincides with strain-stabilized predictions but the two outer lines do not have a strain-stabilized counterpart and are additional resonances. It is necessary therefore to look at zero-strain lines [most probably the result of case (a)] in the region for B close to [111]; Fig. 5 gives the results. From this figure, it can be concluded that zero-strain resonances are important along the high-symmetry [111] direction, but as we move away from [111] they decrease in intensity and therefore cannot be seen. Zero-strain resonances are not seen for \mathbf{B} perpendicular to [111], namely, the (111) plane.

Bearing in mind that no fitting has been undertaken, agreement between the experimental points and theoretical predictions is good for B along [111]. Note that it will be very difficult, if not impossible to predict whether strain-stabilized or zero-strained sites will dominate as intensity calculations must include the following:

(1) For case (a) an evaluation of the maximum of the product of transition intensity as a function of strain and the

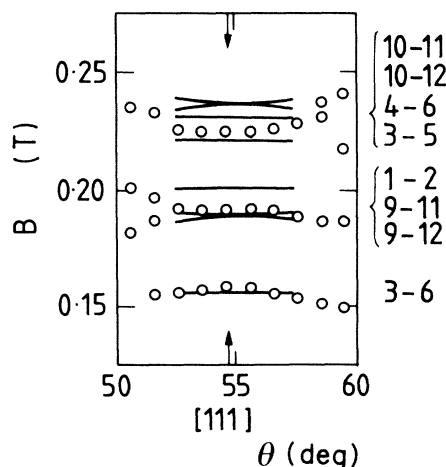


FIG. 5. Experimental data and the zero-strain predictions near [111]. The figure corresponds to the box shown in Fig. 1.

strain distribution function for the crystal.

(2) For case (b) a summation of intensities from all strain-stabilized sites.

For both cases the following must be included:

(3) A summation of electrically and magnetically induced transitions.⁹

(4) An evaluation of the product of intensities of two or more transitions which are close together.

(5) Thermalization. (The exact temperature of the sample is unknown.)

Therefore, we have to allow the experimental spectra to dictate which of case (a) or (b) causes a particular resonance. The intensities of strain-stabilized resonances will depend mainly on the mean width of the strain distribution in the crystal, whereas the intensity resonances around zero strain will depend primarily on the Cr^{3+} concentration, so correlating resonances from different crystals may help experimental identification of the two cases. Note also that this means that the relative intensities of the Cr^{3+} resonances will vary markedly from sample to sample making it difficult to correlate the strength of EPR resonances with the strength of the 1.03-eV ZPL.

If the experimental data are used to determine which case dominates, it can be seen that the fit to that data is excellent in view of the comments above. This is *without any change whatsoever in the parameter values* obtained from optical work. [The fit (6) has been tested with EPR; its predictions are much poorer than for (5)].

Our results and analyses have produced two very significant conclusions. First, we have clearly identified the substitutional Cr^{3+} center in GaP. The main EPR spectra at low fields come from tetragonal sites and the 1.03-eV ZPL and the EPR spectra are both from Cr^{3+} ions. Second, the importance of formulating a dynamic Jahn-Teller model in which strain-stabilized sites often generate the observed symmetry in the EPR spectra is again emphasized as in the case of Cr^{2+} ions in GaAs.¹³ Further theoretical work is in progress to verify the nature of the optical excited state and to explain phonon scattering.¹⁴

The Laboratoire de Physique des Milieux Condensés is a "unité associée au Centre National de la Recherche Scientifique, No. 796."

¹J. J. Krebs and G. H. Stauss, *Phys. Rev. B* **15**, 17 (1977).

²B. Clerjaud, *J. Phys. C* **18**, 3615 (1985).

³B. Clerjaud and A. Gelineau, *Phys. Rev. B* **16**, 82 (1977).

⁴U. Kaufmann and J. Schneider, *Appl. Phys. Lett.* **36**, 747 (1980); N. K. Goswami, R. C. Newman, and J. E. Whitehouse, *Solid State Commun.* **36**, 897 (1980).

⁵C. A. Bates, J. Handley, A. Vasson, and A-M. Vasson, *J. Phys. C* **17**, L603 (1984).

⁶U. Kaufmann and J. Schneider, *Adv. Electron. Electron Phys.* **58**, 81 (1982).

⁷B. Clerjaud, C. Naud, G. Picoli, and Y. Toudic, *J. Phys. C* **17**, 6469 (1984).

⁸P. J. Williams, L. Eaves, P. E. Simmonds, M. O. Henry, E. C.

Lightowers, and Ch. Uihlein, *J. Phys. C* **15**, 1337 (1982); J. Barrau and M. Brousseau (private communication).

⁹M. Rezki, A. Vasson, A-M. Vasson, A. S. Abhavani, and C. A. Bates, *J. Phys. C* **15**, 2207 (1982).

¹⁰L. Eaves, D. P. Halliday, and Ch. Uihlein, *J. Phys. C* **18**, L449 (1985).

¹¹C. A. Bates, *Phys. Rep.* **35**, 187 (1977).

¹²C. A. Hemstreet and J. O. Dimmock, *Phys. Rev. B* **20**, 1527 (1979).

¹³A. S. Abhavani, C. A. Bates, and D. R. Pooler, *J. Phys. C* **17**, 1713 (1984).

¹⁴N. Butler, J. Jouglar, B. Salce, L. J. Challis, and P. L. Vuillermoz, *J. Phys. C* **18**, L731 (1985).